

Performance Analysis of a Co – Flow Planar Anode Supported Solid Oxide Fuel Cell with Internal Reformation

Penyarat Chinda^{1*}, Wisanuruk Wechsato¹, Rapeepong Suwanwarangkul², Somchai Wongwises³
and Juan C. Ordonez⁴

¹Automotive and Alternative Energy Lab (AAA), Department of Mechanical Engineering,
King Mongkut's University of Technology Thonburi, Thungkru, Bangkok 10140, Thailand

²School of Bio-Chemical Engineering and Technology, Sirindhorn International Institute of
Technology,
Thammasart University, Rungsit, Pathum Thani 12121, Thailand

³Fluid Mechanics, Thermal Engineering and Multiphase Flow Research Lab (FUTURE),
Department of Mechanical Engineering, King Mongkut's University of Technology Thonburi,
Thungkru, Bangkok 10140, Thailand

⁴Center of Advanced Power Systems and Department of Mechanical Engineering,
Florida State University, Tallahassee, FL 32310, U.S.A.

Abstract

Solid oxide fuel cells (SOFCs) are an alternative distributed power source due to their high thermal efficiency, low emission and multiple fuel utilization. SOFC can be supplied with various kinds of fuels such as natural gas, carbon monoxide, methanol, ethanol and hydrocarbon compounds. In this study, a mathematical model of a co-flow planar anode supported solid oxide fuel cell with internal reformation of natural gas has been developed in MATLAB code. The model solves simultaneously mass and energy transport equations, chemical as well as electrochemical reactions. The model can predict effectively the temperature and compound specie distributions as well as the SOFC cell performance under specific operating conditions. The cell performance is reported for several operating temperature and pressure. The cell performance is specified in term of cell voltage and power density at any specific current density. The influence of electrode microstructure on cell performance was investigated. The simulation results show that the steady state performance is almost insensitive to microstructure of cells such as porosity and tortuosity. At standard operating pressure (1 atm) and 800 °C with 41% fuel utilization, an output cell voltage of 0.73 volt, a current density of 0.38 A/cm² with a power density of 0.2774 W/cm² was predicted.

Keywords: Solid Oxide Fuel Cells, Co – flow planar anode supported SOFC, Internal reformation, Cell performance, Electrode microstructure

1. Introduction

Solid oxide fuel cells (SOFCs) are an energy conversion device that produces electricity and heat directly from gasified fuels by electrochemical combination of fuels and oxidants. One cell of SOFCs consists of interconnect structures and a three layer region composed of two ceramic electrodes (anode and cathode) separated by a dense ceramic electrolyte. SOFCs operate at high temperature around 600 – 1000 °C [1, 2] and either atmospheric or elevated pressures, while can utilize variety of fuels. Oxygen ions formed at the

Corresponding *e-mail: penyarat@yahoo.com

releasing electrons that flow via an external circuit to the cathode/electrolyte interface. The flexibility in fuel utilization is an advantage of SOFCs over other types of fuel cells. Hydrocarbon fuels can be supplied directly to the SOFCs without the necessary of pre-reformation process, thus diminishing the external reformers [1, 2]. In this work the focus is on the mathematical modeling of SOFC behaviors with direct internal reformation.

The planar SOFC type, which is the focus of this work, provides higher power density than the tubular type [2] due to its shorter current flow path and lower ohmic polarization loss. Moreover, planar SOFC is simpler to fabricate and can be manufactured into various configurations [1, 2].

The problems associated with the high temperature operating condition of planar SOFCs are the internal stress and sealing problem due to non-uniform thermal

expansion caused by non-uniform temperature distribution. To overcome such problems, the operating temperature condition has been reduced to immediate range (roughly around 600-800°C). Thinner electrolytes have been used to reduce the ohmic loss.

In this work anode-supported SOFC type was considered due to its suitable configuration for direct internal reformation of hydrocarbon fuels. Methane was used as the supplied fuel in this study. Reformation process inside the anode is composed of steam-methane reforming reaction and water gas shift reaction [3].

Recently various models of gas transport inside the thick porous anode have been proposed by several researchers. Yakabe et al. [4] and Lehnert et al. [5] applied a mass transport model similar to the dusty-gas model (DGM) in their computational model. Suwanwarangkul et al. [6] compared the accuracy to simulate gas transport phenomena inside anode of three different models: Fick's law model (FM), Stefan – Maxwell model (SMM) and the dusty-gas model (DGM). Among the three models, the dusty gas model provided the most accuracy to predict the gas transport behavior inside anode when compared with the experiment on the mass transport of $H_2 - H_2O - Ar$ and $CO - CO_2$. Unlike the works by Yakabe et al. and Lehnert et al., the water gas shift reaction was omitted in the numerical analysis by Suwanwarangkul et al.

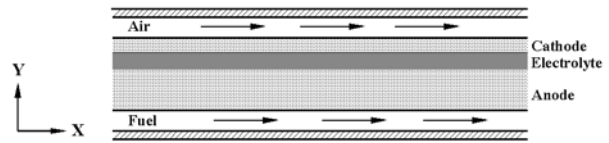
Ackmann et al. [7] applied the mean transport pore model (MTPM) to analyze the mass transport in a two dimensional cell model. They included the effects of chemical and electrochemical reactions on the heat transfer and temperature distribution inside the cell.

In this work, we developed a mathematical model to predict the cell performance of a co-flow planar anode-supported solid oxide fuel cells when natural gas is the supplied fuel. The effects of chemical and electrochemical reactions on the heat and mass transports inside the cell were included in the computational analysis. The concept of optimized partial pre-reformation ratio in direct internal reformation process of natural gas based on the experimental data of Meusinger et al. [8] was introduced to prevent excessive temperature gradient across the cell. The mass transport in gas flow channels is considered as mass convection, while the mass transport inside the porous electrodes is considered as mass diffusion. The heat transfer model is included of convective heat transfer between solid and gas phase as well as conductive heat transfer in solid cell components. The endothermic heat consumed during the steam - methane reforming and the exothermic heat released from the electrochemical reactions were included as the heat sources in the numerical calculation of temperature distribution.

2. Mathematical Modeling

The supplied natural gas to the anode was assumed to have the following compositions: 87% by mole of CH_4 , 6% by mole of C_2H_6 and 2% by mole of higher hydrocarbon with 30% pre-reformation following suggestion by Meusinger et al. [8]. Air supplied to the

cathode was used as the oxidant. All gases behave as ideal gases. The electrodes have homogeneous and isotropic structures. Mass transport in porous electrode is considered as mass diffusion accompanied by chemical and electrochemical reactions. Steam reforming reaction is assumed to occur at the surface of anode and water-gas shifted reaction is assumed to occur inside the void volume of anode. The electrochemical reaction occurs at the vicinity area of anode and electrolyte interface. Fully developed gas flowing through channels is considered as incompressible in laminar flow regime due to its low velocity. Mass transport in gas flow channels were considered mainly as pure mass convection. A schematic one dimensional model of a co-flow planar anode-supported solid oxide fuel cell is shown in Fig. 1. Air and fuel enter the cell in the same direction via the flow channels and diffuse through the porous void of the electrodes (cathode and anode). The dimension of cell components and standard parameters used in calculation are given in Table 1.



All dimensions not to scale

Figure 1 one dimensional model of a co-flow planar anode-supported SOFC

Table 1 Standard parameters used in this study

| Geometrical parameters of the cell | |
|---|---|
| Anode thickness | 2 mm. |
| Anode length | 10 cm. |
| Anode porosity (ϵ) | 0.4 |
| Anode tortuosity (τ) | 2.75 |
| Anode pore radius (r_{an}) | 1 μm . |
| cathode thickness | 60 μm . |
| cathode length | 10 cm. |
| cathode porosity (ϵ) | 0.4 |
| cathode tortuosity (τ) | 2.75 |
| cathode pore radius (r_{ca}) | 1 μm . |
| electrolyte thickness | 60 μm . |
| electrolyte length | 10 cm. |
| Chemical and electrochemical parameters | |
| transfer coefficient (α) | 0.5 |
| cathode exchange current density (j_{oc}) | 0.1×10^4 [A/m ²] |
| anode exchange current density (j_{oa}) | 1×10^4 [A/m ²] |
| cathode limiting current density ($j_{lim,c}$) | 1×10^5 [A/m ²] |
| electrolyte constant (A) | 9×10^7 [K/ohm*m] |
| electrolyte activation energy (G_{act}) | 100×10^3 [J/mol] |
| faraday constant (F) | 96485 C/mole |
| specific surface area (A_s) | 3×10^6 [m ² /m ³] |
| Thermal parameters | |
| anode effective thermal conductivity ($\lambda_{eff,an}$) | 3 [W m ⁻¹ K ⁻¹] |

| | |
|---|--|
| anode convective heat transfer coefficient (h_{an}) | 57 [W m ⁻² K ⁻¹] |
| cathode effective thermal conductivity ($\lambda_{eff,cat}$) | 3.8 [W m ⁻¹ K ⁻¹] |
| cathode convective heat transfer coefficient (h_{cat}) | 49 [W m ⁻² K ⁻¹] |
| electrolyte effective thermal conductivity ($\lambda_{eff,elec}$) | 1.8 [W m ⁻¹ K ⁻¹] |
| Flow rate of fuel and air at the inlet | |
| fuel flow rate | 0.5x10 ⁻³ m ³ /min |
| air flow rate | 5x10 ⁻³ m ³ /min |
| Operating pressure and temperature of the cell | |
| operating pressure (P) | 1 atm |
| operating temperature (T) | 800 °C |

2.1 Mass transport

Mass transport in a solid oxide fuel cell composed of 2 parts, mass diffusion in porous electrodes and mass convection in gas flow channels. Since the cathode is relatively thin comparable to the anode thickness, the mass diffusion in the cathode side could be omitted in this computational analysis.

Mass balance in porous anode

The gas transport within the anode pores, which is strongly dependent on the anode microstructure, can be described by combining the Stefan–Maxwell and Knudsen diffusion relations. By assuming that the total pressure is uniform throughout the porous anode, the mass diffusive flux through the anode can be deduced as in Eq. 1,

$$\frac{N_i}{D_{i,k}^{eff}} + \sum_{j=1, j \neq i}^n \frac{y_j N_i - y_i N_j}{D_{ij}^{eff}} = -\frac{P}{RT} \left(\frac{dy_i}{dy} \right) \quad (1)$$

where y_i is the mole fraction, P is pressure and T is temperature, while N_i and N_j are the molar flux of species i and j, respectively. $D_{i,k}^{eff}$ is the effective Knudsen diffusion coefficient and D_{ij}^{eff} is the effective diffusion coefficient.

The effective diffusion coefficient through the porous electrode can be calculated from

$$D_{i,j}^{eff} = \psi D_{ij} \quad \text{or} \quad D_{i,j}^{eff} = (\varepsilon^{1.5}) D_{ij} \quad (2)$$

The Knudsen diffusion coefficient ($D_{i,k}$) and the effective Knudsen diffusion ($D_{i,k}^{eff}$) coefficient for gas specie i can be calculated by Eqs. (3) and (4), respectively [9, 10].

$$D_{i,k} = \frac{2}{3} \bar{r} \sqrt{\frac{8RT}{\pi M_i}} \quad (3)$$

$$D_{i,k}^{eff} = \psi D_{i,k} \quad (4)$$

where ψ is the ratio between the porosity and tortuosity and M_i is the molecular weight of specie i.

The mass balance of all species i in the porous anode where both mass diffusion and chemical reactions occur is

$$\frac{\psi}{RT} \frac{d(y_i P)}{dt} = -\nabla \cdot N_i + r_i \quad (5)$$

Two types of chemical reactions (methane-steam reforming and water-gas shifted reactions) occur at anode during supplying the fuel cells with natural gas.



The endothermic methane-steam reforming reaction occurs at the surface of anode while the exothermic water-gas shift reaction occurs in the porous void volume of anode. The reaction rate of methane-steam reforming reaction and water-gas shifted reaction can be determined from Arrhenius' curve fits of the data reported by Lehnert et al. [5, 11] as in Eqs. (8)-(11),

$$R_1 = k_{rf} \left(P_{CH_4} P_{H_2O} - \frac{(P_{H_2})^3 P_{CO}}{K_{pr}} \right) \quad [\text{mol m}^{-3} \text{s}^{-1}] \quad (8)$$

$$k_{rf} = 2395 \exp\left(-\frac{231266}{RT}\right) \quad [\text{mol m}^{-3} \text{Pa}^{-2} \text{s}^{-1}] \quad (9)$$

$$R_2 = k_{sf} \left(P_{H_2O} P_{CO} - \frac{P_{H_2} P_{CO_2}}{K_{ps}} \right) \quad [\text{mol m}^{-3} \text{s}^{-1}] \quad (10)$$

$$k_{sf} = 0.0171 \exp\left(-\frac{103191}{RT}\right) \quad [\text{mol m}^{-3} \text{Pa}^{-2} \text{s}^{-1}] \quad (11)$$

where R_1 is the reaction rate of methane-steam reforming reaction and R_2 is the reaction rate for water-gas shifted reaction, k_{rf} is the forward catalyzed reaction rate constant of the reforming reaction and k_{sf} is the forward catalyzed reaction rate constant of the water-gas shifted reaction. The parameter R is the universal gas constant. K_{pr} is the equilibrium constant for the steam reforming reaction and K_{ps} is the equilibrium constant for the water-gas shifted reaction [11]. Both constants can be calculated from

$$K_{pr} = 1.0267 * 10^{10} * \exp(-0.2513Z^4 + 0.3665Z^3 + 0.5810Z^2 - 27.134Z + 3.2770) \text{Pa}^2 \quad (12)$$

$$K_{ps} = \exp(-0.2935Z^3 + 0.6351Z^2 + 4.1788Z + 0.3169) \quad (13)$$

$$Z = \frac{1000}{T(K)} - 1 \quad (14)$$

The molar specie formation rate, r_i in Eq. (5) can be calculated from Eqs. (15) – (19). The minus sign refers to the consuming rate of each species, while the plus sign refers to the production rate.

$$r_{CH_4} = -R_1 \quad [\text{mol m}^{-3} \text{ s}^{-1}] \quad (15)$$

$$r_{H_2O} = -R_1 - R_2 \quad [\text{mol m}^{-3} \text{ s}^{-1}] \quad (16)$$

$$r_{CO} = R_1 - R_2 \quad [\text{mol m}^{-3} \text{ s}^{-1}] \quad (17)$$

$$r_{H_2} = 3R_1 + R_2 \quad [\text{mol m}^{-3} \text{ s}^{-1}] \quad (18)$$

$$r_{CO_2} = R_2 \quad [\text{mol m}^{-3} \text{ s}^{-1}] \quad (19)$$

The current density from the electrochemical reaction of hydrogen can be calculated by Faraday's law.

$$N_{H_2} = \frac{j}{2 \cdot F} \quad (20)$$

$$N_{H_2O} = -\left(\frac{j}{2 \cdot F}\right) \quad (21)$$

Mass balance in gas flow channels

The mole fraction of each gas specie changes along the flow channels length due to the normal molar flux N_i in y direction through the porous electrodes. For steady state, mass balance for each specie i can be deduced as in Eq. (22). Note that the pressure drop along the flow channels is assumed negligible.

$$\frac{dF_i}{dx} = 2\pi X v_i N_{i(y=0)} \quad (22)$$

where F_i is the molar flow rate for specie i and v_i is the stoichiometric coefficient (-1 for reactant species and +1 for product species).

2.2 Heat transfer within the cell

The heat transfer in the porous electrodes and dense electrolyte is dominated by conduction,

$$\lambda^{eff} \left(\frac{\partial^2 T}{\partial x^2} + \frac{\partial^2 T}{\partial y^2} \right) + q = 0 \quad (23)$$

where q is the heat source term reflecting both exothermic and endothermic reactions. The effective thermal conductivity coefficient (λ^{eff}) consists of a solid conductive coefficient (λ_s) and a gas conductive coefficient (λ_f),

$$\lambda^{eff} = \varepsilon \lambda_f + (1 - \varepsilon) \lambda_s \quad (24)$$

The heat source term is related to the chemical reactions within porous anode and the electrochemical reaction at the electrode-electrolyte interface Heat consumed during the methane-steam reformation at the surface of anode is

$$q_1 = R_1 \cdot A_s \cdot (-\Delta H_1^\circ) \quad (25)$$

Heat released during the water-gas shifted reaction in the void volume of anode is

$$q_2 = R_2 \cdot \varepsilon \cdot (-\Delta H_2^\circ) \quad (26)$$

Heat release from the electrochemical reaction at electrode-electrolyte interface is

$$q_3(x) = \frac{j(x)}{2F} \Delta H_{H_2O} + j(x) \cdot V_C \quad (27)$$

where A_s is the specific surface area (area per volume ratio), ε is the porosity and ΔH is the enthalpy of formation.

Heat transfer at the interface between the gas flow channels and the electrode is pure convection

$$q_{conv,i} = h_i (T_i - \bar{T}_{c,i}) \quad (28)$$

where h_i is the convective heat transfer coefficient of specie i. The temperature term $\bar{T}_{c,i}$ is the average temperature along the flow channels. The temperature T_i is the surface temperature of the electrode. All temperatures are introduced to the mass balance models in order to calculate the chemical kinetic constants.

2.3 Cell electrical performance

The cell voltage V_C is assumed constant along the cell length and can be calculated by potential balance,

$$V_C = E_{j=0} - (\eta_{ohmic} + \eta_{conc,a} + \eta_{conc,c} + \eta_{act,a} + \eta_{act,c}) \quad (29)$$

where $E_{j=0}$ is the open circuit voltage and can be calculated from Nernst's equation,

$$\begin{aligned} E &= -\frac{\Delta G^\circ}{2F} - \frac{RT}{2F} \ln \left(\frac{P_{H_2O}^a}{P_{H_2}^a (P_{O_2}^c)^{1/2}} \right) \\ &= E^\circ + \frac{RT}{4F} \ln \left(\frac{P_{O_2}^c (P_{H_2}^a)^2}{(P_{H_2O}^a)^2} \right) \end{aligned} \quad (30)$$

where ΔG° is the net standard Gibbs free energy of electrochemical reaction at 1 atm and 25 °C, E° is the standard Nernst potential at 1 atm and 25 °C, $P_{H_2O}^a$ is the water partial pressure, $P_{H_2}^a$ is the hydrogen partial pressure and $P_{O_2}^c$ is the oxygen partial pressure.

The parameter η_{ohmic} is ohmic polarization loss. In SOFCs, ohmic polarization in anode and cathode is assumed to be negligible, hence the ohmic polarization is only related to the electrolyte resistance. η_{conc} is the

concentration polarization and η_{act} is the activation polarization. Therefore the ohmic polarization based the electrolyte resistance can be determined from [12]

$$\eta_{ohmic} = j(ASR_{ohmic}) = j \cdot \left(\frac{t^E}{\sigma} \right) \quad (31)$$

where t^E is the thickness of the electrolyte. The electrolyte conductivity (σ) can be calculated from,

$$\sigma = \frac{A \cdot \left(e^{-\Delta G_{act} / (RT)} \right)}{T} \quad (32)$$

where A is the electrolyte constant and ΔG_{act} is the electrolyte activation energy.

In case of SOFCs with thick anode, the anodic concentration or anodic diffusive polarization can be expressed from the Nernst's equation as [13],

$$\eta_{conc,a} = \frac{RT}{2F} \ln \left(\frac{y_{H_2} y_{H_2O}^o}{y_{H_2}^o y_{H_2O}} \right) \quad (33)$$

where y_i and y_i^o represent the mole fractions at nonzero and zero current densities at the anode-electrolyte interface. The cathodic concentration polarization is expressed as [13]

$$\eta_{conc,c} = \frac{RT}{2F} \ln \left(1 - \frac{j}{j_{lim,c}} \right) \quad (34)$$

where $j_{lim,c}$ is the cathode limiting current density.

The activation polarization terms are related to the electrochemical reactions rate. The activation polarization terms located at the electrode-electrolyte interface can be calculated from the Butler-Vollmer equation [13]. The anodic and cathodic activation polarization losses are expressed respectively as,

$$\eta_{act,a} = \frac{RT}{F} \operatorname{arcsinh} \left(\frac{j}{2 \cdot j_{0,a}} \right) \quad (35)$$

$$\eta_{act,c} = \frac{RT}{F} \operatorname{arcsinh} \left(\frac{j}{2 \cdot j_{0,c}} \right) \quad (36)$$

where $j_{0,a}$ and $j_{0,c}$ are respectively the anodic and cathodic current densities at which the overvoltage begins to move from zero [1].

The Runge-Kutta method was used to solve mass diffusion equations coupled with the heat transfer equations. The molar fraction of specie i at $y_i(x, y = 0)$ is equal to the molar fraction in the gas flow channels. At y equal to the anode thickness t^A , the mass flux N_i is zero for CH_4 , CO and CO_2 , while N_i is given by the Faraday's law Eqs. (20) - (21) respectively for H_2 and H_2O . The

numerical iteration is repeated until the predicted current density agrees with the corresponding current density to the specified cell voltage (V_C) in Eq. (29).

3. Results and Discussion

The developed model can be used to investigate the effect of operating conditions and design parameters, especially the geometry of electrode microstructures on the performance of a co-flow planar anode supported SOFC.

The effect of operating temperature on the cell current density and voltage is reported in Fig. 2. The effect of temperature on the cell power density and voltage is reported in Fig. 3. The cell operating pressure is at 1 atm.

Figure 2 shows that at zero current density, the open circuit voltage decreases as temperature increases; whereas the current density increases, the cell voltage increases with the operating temperature of the cell. Increase in operating temperature not only enhances the rate of electrochemical reaction, but also increases the rate of ionic conductivity, which in turn minimizes the ohmic contribution to the polarization loss and thus enhances the cell voltage and cell power density as shown respectively in Figs. 2 and 3. The mathematical model predicted that the maximum power density of the cell about 0.2774 W/cm^2 is given at the current density of 0.38 A/cm^2 and cell voltage of 0.73 volt when the cell is operated at the standard pressure of 1 atm and temperature of $800 \text{ }^\circ\text{C}$. The fuel utilization is at 41 percent.

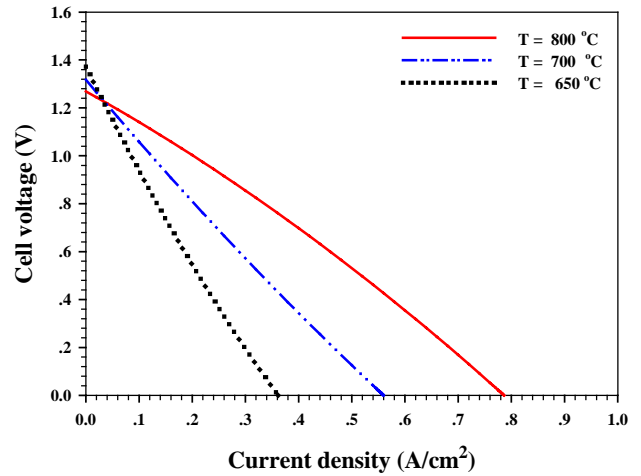


Figure 2 Effect of temperature on cell voltage and current density

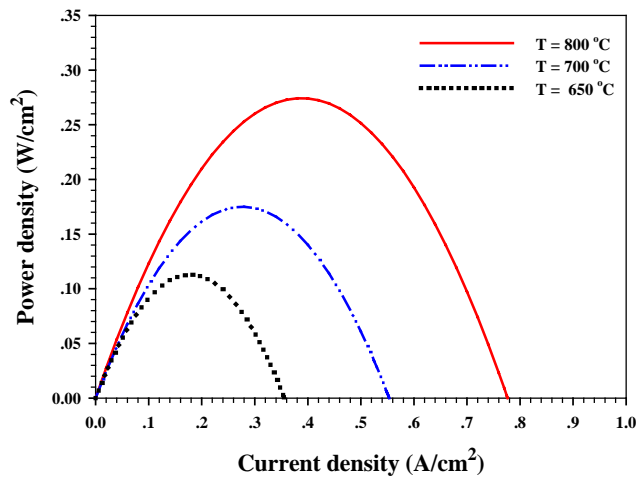


Figure 3 Effect of temperature on cell power density and current density

Figures 4 and 5 show the effects of pressure on the cell voltage and on power density at the specified current density respectively. Both cell voltage and power density increase with the operating pressure due to the increase in reactant concentration. However, increase in operating pressure may result in gas sealing problems [1].

In order to study the effects of cell geometry such as porosity, tortuosity, pore-radius and electrolyte thickness on the cell performance, the operating condition is set at 800 °C and 1 atm. The effects of porosity on cell voltage and on power density at the specified current density are shown respectively in Figs. 6 and 7. The cell voltage and power density only increases with the porosity at high current density. Normally the concentration polarization loss decreases, while the ohmic polarization loss increases as the porosity increases. This implies that the concentration polarization loss is the dominant loss at high current density.

The effects of tortuosity on the cell performance are reported in Figs. 8 - 9. As the tortuosity increases the specie diffusion rate decrease; hence the reaction rate decreases causing the cell voltage and power density to decrease.

The effects of the pore-radius on the single cell

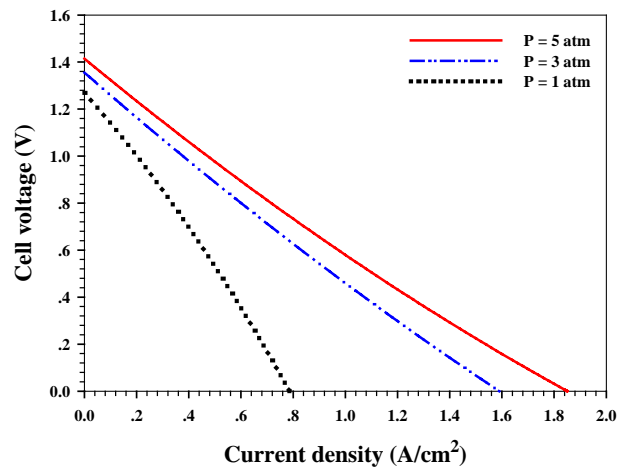


Figure 4 Effect of pressure on cell voltage

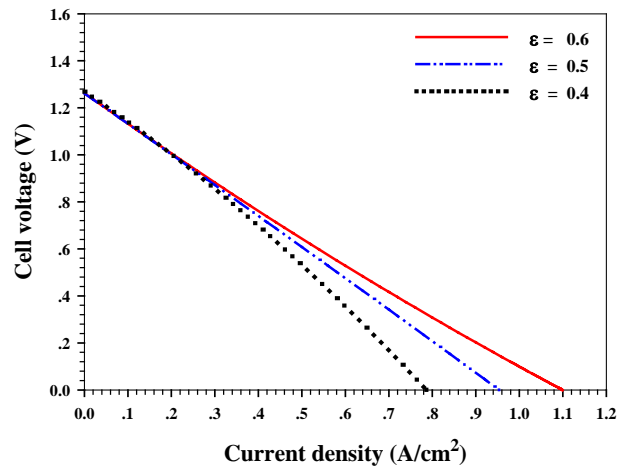


Figure 6 Effect of porosity on cell voltage performance are reported in Figs. 10 – 11. As the pore size increases, the specie diffusion resistance decreases; thus the cell voltage and the power density increase.

Figures 12 -13 show the effects of electrolyte thickness on the cell performance. The cell voltage and power density at a specified current density increase as the electrolyte thickness decreases due to the decrease in ohmic loss.

4. Conclusions

A mathematical model for predicting the performance of a co-flow planar anode supported solid oxide fuel cell with internal reformation of natural gas was developed in MATLAB code. The model solved simultaneously mass and energy transport equations as well as chemical and electrochemical reactions. The model can predict the cell performance at various operating conditions. The model is useful in analyzing the effects of porosity, tortuosity and pore radius on the cell performance. The performance of the cell was reported in terms of cell voltage and power density at specified

current densities for several operating temperature and pressure.

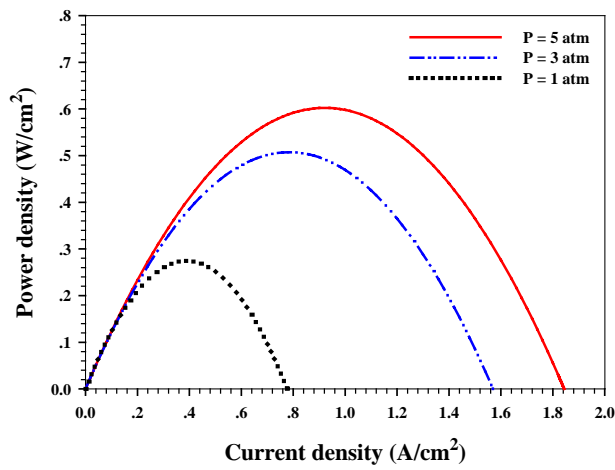


Figure 5 Effect of pressure on cell power density

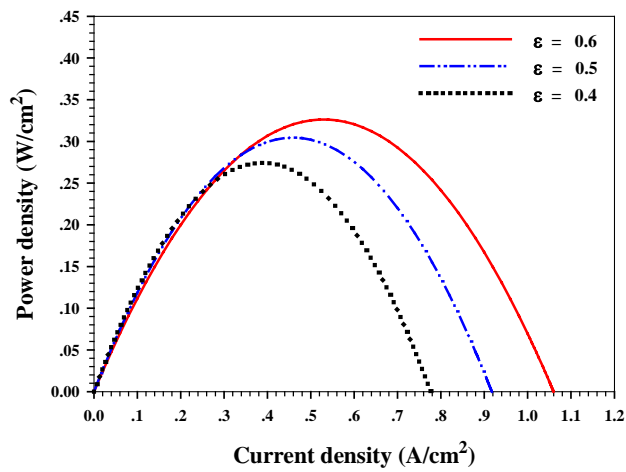


Figure 7 Effect of porosity on cell power density

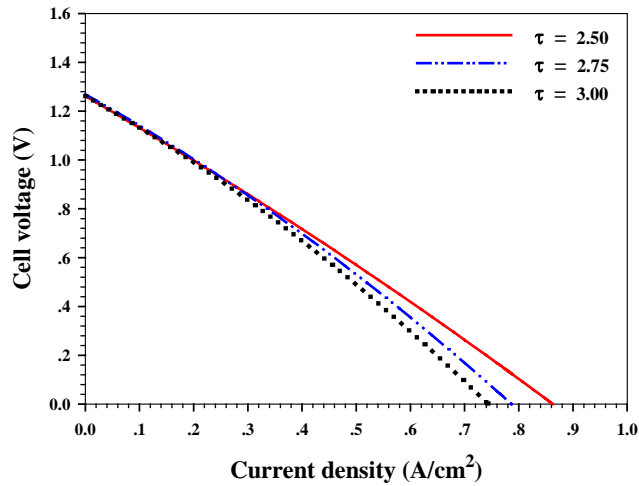


Figure 8 Effect of tortuosity on cell voltage

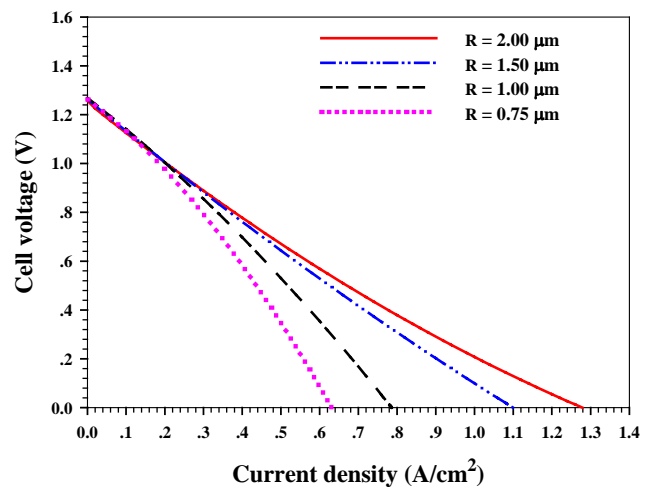


Figure 10 Effect of pore radius on cell voltage

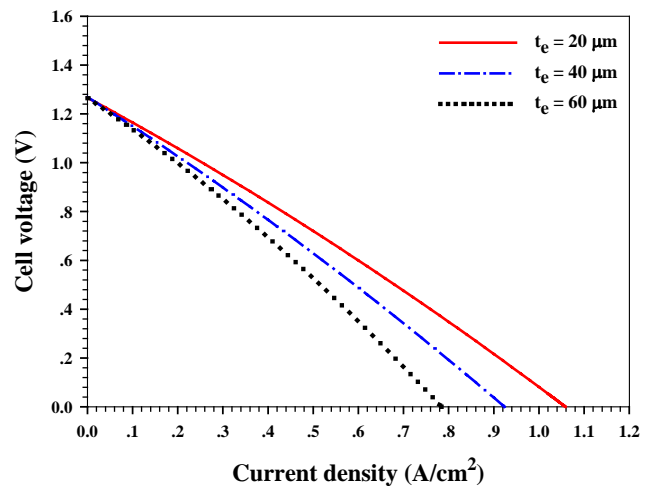


Figure 12 Effect of electrolyte thickness on cell voltage

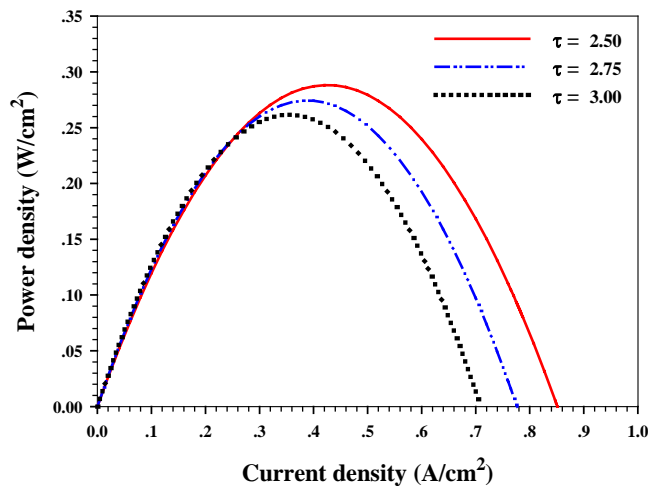


Figure 9 Effect of tortuosity on cell power density

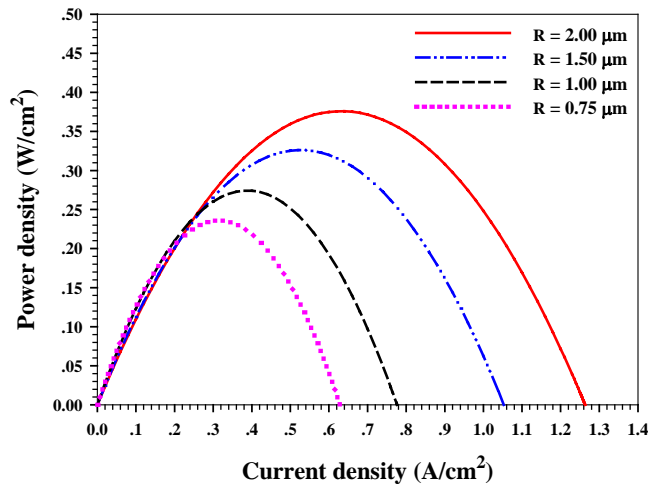


Figure 11 Effect of pore radius on cell power density

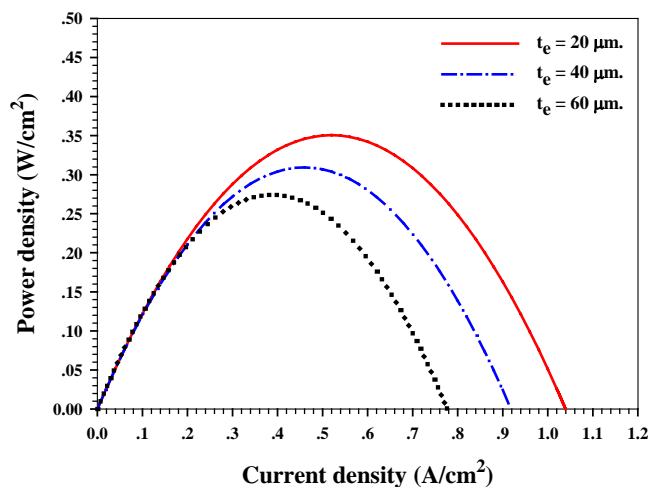


Figure 13 Effect of electrolyte thickness on cell power density

Acknowledgement

Authors would like to acknowledge with sincere gratitude to the Thailand Research Fund for providing the financial support.

References

- [1] Singhal, S.C., and Kendall, K., 2003. High Temperature Solid Oxide Fuel Cells : Fundamentals Design and Applications. Elsevier Ltd, Oxford, U.K.
- [2] Larminie, J., and Dicks, A., 2000. Fuel Cell Systems Explained. John Wiley and Sons Ltd, Chichester
- [3] Aguiar, P., Adjiman, C.S. and Brandon, N.P., 2004. Anode – Supported Intermediate Temperature Direct Internal Reforming Solid Oxide Fuel Cell I: model based steady - state. Journal of Power Sources, Vol. 138, pp. 120-136
- [4] Yakabe, H., Hishinuma, M. Uratani, M., Matsuzaki, Y., and Yasuda, I. 2000. Evaluation and Modeling of Performance of Anode – Supported Solid Oxide Fuel Cell. Journal of Power Sources, Vol. 86, pp. 423-431
- [5] Lehnert, W., Meusinger, J., and Thom, F., 2000. Modeling of Gas Transport Phenomena in SOFC Anodes. Journal of Power Sources, Vol. 87, pp. 57-63
- [6] Suwanwarangkul, R., Croiset, E., Fowler, M.W., Douglas, P.L., Entchev, E., and Douglas, M.A., 2003. Performance Comparison of Fick's, Dusty – gas and Stefan – Maxwell Models to Predict the Concentration Overpotential of a SOFC Anode. Journal of Power Sources, Vol. 122, pp. 9- 18
- [7] Ackmann, T., De Haart, L. G. J., Lehnert, W. and Stolten, D., 2003. Modeling of Mass and Heat Transport in Planar substrate Type SOFCs. Journal of the Electrochemical Society, Vol. 150(6), pp. A783-A789
- [8] Meusinger, J., Riensche, E. and Stimming, U., 1998. Reforming of Natural Gas in Solid Oxide Fuel Cell Systems. Journal of Power Sources, Vol. 71, pp. 315-320
- [9] Bird, R.B., Stewart, W.E. and Lightfoot, E.N., 2001. Transport Phenomena., Second edition, John Wiley and Sons, New York, U.S.A.
- [10] Tod, B., and Young, J.B., 2002., Thermodynamics and Transport Properties of Gases for Use in Solid Oxide Fuel Cell Modeling., Journal of Power Sources, Vol. 110, pp. 186-200
- [11] Haberman, B.A., and Young, J.B., 2004., Three – Dimensional Simulation of Chemically Reacting Gas Flows in the Porous Support Structure of an Integrated-Planar Solid Oxide Fuel Cell., International Journal of Heat and Mass Transfer, Vol. 47, pp. 3617-3629
- [12] Hayre, R.O., Won Cha, S., Colella W. and Prinz, F. B., 2006. Fuel Cell Fundamentals., John Wiley and Sons, New York, U.S.A.
- [13] Morel, B., Laurencin, J., Bultel, Y. and Lefebvre-Joud, F., 2005., Anode – Supported SOFC Model

Centered on the Direct Internal Reforming., Journal
of the Electrochemical Society, Vol. 152(7), pp.
A1382-A1389